Journal of Vacuum Science and Technology A

RESEARCH ARTICLE | MARCH 11 2024

Inhibition of atomic layer deposition of TiO_2 by functionalizing silicon surface with 4-fluorophenylboronic acid

Special Collection: Atomic Layer Deposition (ALD)

Dhamelyz Silva-Quinones ; John R. Mason ; Robert Norden ; Andrew V. Teplyakov

J. Vac. Sci. Technol. A 42, 032402 (2024)
https://doi.org/10.1116/6.0003316

JVST A
Journal of Vacuum Science & Technology A

ARTICLE

pubs.aip.org/avs/jva

Inhibition of atomic layer deposition of TiO_2 by functionalizing silicon surface with 4-fluorophenylboronic acid

Cite as: J. Vac. Sci. Technol. A 42, 032402 (2024); doi: 10.1116/6.0003316
Submitted: 21 November 2023 · Accepted: 9 February 2024 ·
Published Online: 11 March 2024

Dhamelyz Silva-Quinones, John R. Mason, Robert Norden, and Andrew V. Teplyakov[a)]

AFFILIATIONS

Department of Chemistry and Biochemistry, University of Delaware, Newark, Delaware 19716

Note: This paper is part of the 2024 Special Topic Collection on Atomic Layer Deposition (ALD).
[a)]**Author to whom correspondence should be addressed:** andrewt@udel.edu

ABSTRACT

As the size of the components in electronic devices decreases, new approaches and chemical modification schemes are needed to produce nanometer-size features with bottom-up manufacturing. Organic monolayers can be used as effective resists to block the growth of materials on non-growth substrates in area-selective deposition methods. However, choosing the appropriate surface modification requires knowledge of the corresponding chemistry and also a detailed investigation of the behavior of the functionalized surface in realistic deposition schemes. This study aims to investigate the chemistry of boronic acids that can be used to prepare such non-growth areas on elemental semiconductors. 4-Fluorophenylboronic acid is used as a model to investigate the possibility to utilize the Si(100) surface functionalized with this compound as a non-growth substrate in a titanium dioxide (TiO_2) deposition scheme based on sequential doses of tetrakis(dimethylamido) titanium and water. A combination of X-ray photoelectron spectroscopy and time-of-flight secondary ion mass spectrometry allows for a better understanding of the process. The resulting surface is shown to be an effective non-growth area to TiO_2 deposition when compared to currently used H-terminated silicon surfaces but to exhibit much higher stability in ambient conditions.

I. INTRODUCTION

Modern requirements for microelectronic devices to be developed past Moore's law into the so-called more-than-Moore direction[1] require both miniaturization of the device features and exceptional conformality, which can only be delivered by bottom-up self-aligned nanofabrication. This approach is rooted in area-selective atomic layer deposition or area-selective deposition techniques that have become the subject of intense research in recent years.[2,3] They address the challenge of limiting the growth in specific areas by taking advantage of the differences in local surface chemistry. In other words, by changing the surface reactivity of the substrate one can favor or prevent the growth of a specific material on the target surface.[3–5] Thus, the growth is expected on the growth area (GA) where the surface is modified using promotor-type molecules but delayed or avoided on the non-growth area (NGA) where the surface is modified using inhibitor-type molecules so that atomic level accuracy can be achieved.[6] The measure of efficiency of this difference in reactivity is characterized by selectivity, which is discussed later.

Although sometimes combinations of GA and NGA with high intrinsic selectivity can be utilized directly as prepared, most of the time, the intricate patterns used for modern applications and especially for 3D components, require some sort of chemical patterning, where passivated areas serve as NGA. In the past, polymer masks and self-assembled monolayers of functional alkyl molecules were used with a high degree of success;[7–12] however, with the size of the target features quickly approaching single nanometer scale, the need for alternative materials for surface modification became apparent. In silicon-based production, the most common approach is to use H-terminated silicon surface for patterning that can be achieved with as high resolution as a single atom (with scanning tunneling microscopy) or alternative atomic monolayer systems (Cl^-, Br^-, I^-)[13] but stability of these systems and the difficulty to prepare them consistently outside expensive ultrahigh vacuum conditions brought up a demand for a compromise of the use of small

molecule inhibitors (SMIs),[7] with dimensions of just a few angstroms. SMIs can be introduced right in the midst of the deposition cycle to refresh the NGA and suppress the defects appearing during the deposition. However, the same general strategy can be applied to create an NGA at the start of the deposition process. There are certain requirements for the design and the selection of a good SMI for this purpose. They include chemical stability on a specific surface, steric hindrance, strength of adsorption, preferably fast attachment reaction kinetics, and a minimal number of various binding modes, but most importantly, increased selectivity between GA and NGA.[14]

The 4-fluorophenylboronic acid (FPBA) molecule can be a promising SMI that follows the aforementioned requirements. The chemical reaction of the FPBA with chlorine-terminated silicon surface follows the general condensation scheme, when a chemical functionality of the incoming molecule combines with the surface functionality to produce a stable chemical bond and to release a side product. Similar processes have been demonstrated previously for introducing nitrogen-containing functionalities to silicon by reacting nitro- or nitroso-compounds with H-terminated silicon surfaces with water as a side product[15,16] and for amines reacting with Cl-terminated silicon surfaces releasing hydrochloric acid (HCl) as a side product.[17,18] Not only does FPBA form a condensation product with Cl-terminated silicon releasing HCl, but this reaction is also highly selective compared to the H-terminated silicon surfaces.[19] It leads to the formation of very stable bidentate species with two Si–O–B bonds, which allows for the passivation of the surface and prevents further oxidation.[19] In addition, the FPBA molecule has boron and fluorine elements, which can serve as perfect spectroscopic labels.

This paper will demonstrate that FPBA on silicon forms a stable passivated surface that efficiently inhibits the deposition of titanium dioxide (TiO_2) in an ALD process based on sequential tetrakis(dimethylamido)titanium (TDMAT) and water doses for up to 20 cycles with up to 70% selectivity. This selectivity is nearly identical to that of H-terminated silicon reacted under the same conditions, but the FPBA-terminated surface is exceptionally stable, even in ambient. A detailed spectroscopic investigation confirms the formation of a stable monolayer, and ToF-SIMS profiles of this surface after the eventual loss of selectivity (covered with TiO_2 layer) confirm that the starting substrate is still intact and even identifies the differences in F and B positions at the interface.

II. EXPERIMENT

A. Materials

In this study, single-side polished Si(100) wafers (p-doped, Virginia Semiconductors, 400 ± 25 mm, 1–10 Ω cm resistivity) were used as substrates. The de-ionized water used in all the experiments was from a first-generation Milli-Q water system (Millipore) with 18 MΩ cm resistivity. The chemicals used were reagent grade or better: hydrogen peroxide (Fisher, 30% certified ACS grade), ammonium hydroxide (Fisher, 29% certified ACS grade), hydrochloric acid (Fisher, 37.3% certified ACS grade), Buffered oxide etchant (BOE) 6:1 (Fischer chemical), chlorobenzene (99+%, Acros), phosphorus pentachloride (≥98.0% Sigma-Aldrich), Luperox A75 benzoyl peroxide (75% Millipore Sigma), 4-fluorophenylboronic acid (≥95.0% Sigma-Aldrich), and toluene (Fisher, 99.9% certified ACS). Nitrogen gas used for purging and drying samples was from the boil-off of the liquid nitrogen tank.

B. Preparation procedures

1. Preparation of hydrogen-terminated Si(100) and hydroxyl-terminated surfaces

The Si(100) wafers were cleaned by a modified Radio Corporation of America (RCA) method.[20] The first step is to clean the Teflon beakers with a freshly prepared standard cleaning-1 (SC-1) solution prepared by mixing Milli-Q water, hydrogen peroxide, and ammonium hydroxide (volume ratio 4:1:1) for 30 min on an 80 °C water bath. Second, the silicon wafers were cleaned with another freshly prepared SC-1 solution for 10 min in an 80 °C water bath. Following this step, the silicon wafers were rinsed with Milli-Q water. The clean Si wafers were then etched in an HF buffer solution for 2 min and rinsed again with Milli-Q water. Third, the wafer samples were placed in a freshly prepared standard cleaning-2 (SC-2) solution prepared by mixing Milli-Q water, hydrogen peroxide, and hydrochloric acid (volume ratio 4:1:1) for 10 min in a water bath at 80 °C, this step is used to produce a hydroxyl-terminated surface [OH–Si(100)]. Lastly, the rinsed silicon substrates were etched a second time in HF buffer solution for 1 min, followed by a 6-min etching in ammonium fluoride solution, to form a H–Si(100) surface. The H–Si(100) was then briefly re-dipped in HF and dried before being placed into the commercial ALD.

2. Preparation of chlorine-terminated Si(100) surface

The chlorine-terminated surfaces were prepared by a previously described procedure using PCl_5.[21] The freshly prepared H–Si(100) sample (described in Sec. II B 1) was briefly rinsed in chlorobenzene before being reacted with a solution of phosphorus pentachloride dissolved in chlorobenzene solvent, and benzoyl peroxide was used in trace amounts as a radical initiator. Before starting the reaction, this PCl_5 solution was purged with nitrogen gas for at least 30 min to remove gaseous impurities. The reaction of the PCl_5 solution with the freshly prepared H–Si(100) was carried out in an oil bath at 110 °C for 1 h to form the Cl–Si(100) sample.

3. Reaction of 4-fluorophenylboronic acid with the Cl–Si(100) surface

The freshly prepared Cl–Si(100) sample (described in Sec. II B 2) was rinsed with toluene before being reacted with a solution of FPBA dissolved in toluene (30 mM). Before starting the reaction, the FPBA powder was dissolved in the toluene solvent for 1h at 100 °C under nitrogen stream. The reaction with the FPBA solution and the freshly prepared Cl–Si(100) was carried out on an oil bath at 50 °C for 3h under nitrogen stream, as described previously.[19]

4. Atomic layer deposition of TiO_2 on 4-fluorophenylboronic acid-modified Si(100) and OH–Si(100)

The freshly prepared samples were placed in a commercial Oxford FlexAL II Thermal/Plasma ALD chamber immediately after

the surface modifications in solution described above. The base pressure in the ALD chamber was 7×10^{-9} Torr and the TiO_2 thermal ALD recipe consisted of TDMAT dose for 1 s, 10 s argon (Ar) purge, 60 s vacuum pumping, H_2O dose at 20 ms, Ar purge, and vacuum pumping. The temperature was maintained at 130 °C with a background pressure of 80 mTorr. The reactants were delivered in an Ar carrier gas at 200 SCCM, and purges were performed for 10 s with 100 SCCM Ar. TiO_2 was deposited onto FPBA–Si (100) and OH–Si(100) for 5, 10, 15, 20, 30, 50, and 200 cycles and onto H–Si(100) for 5, 10, 15, 20, 30, and 50 cycles.

C. Characterization techniques

1. X-ray photoelectron spectroscopy (XPS)

The XPS analysis of the samples was performed on a Thermo Scientific K-Alpha+ instrument equipped with an Al Kα source (hν = 1486.6 eV). The base pressure in the XPS chamber was 3.75×10^{-9} Torr and the take-off angle was 35.3° with respect to the analyzer. The survey spectra were collected over a binding energy range of 0–1000 eV, with a pass energy of 200 eV, a step size of 1 eV, and a dwell time of 10 ms. The high-resolution spectra for each element, C 1s, O 1s, B 1s, Si 2p, Cl 2p, F 1s, and Ti 2p, were collected with a pass energy of 50 eV, a step size of 0.1 eV, and a dwell time of 50 ms. The data analysis was processed with CASAXPS software (version 2.3.25). The C 1s peak at 284.6 eV was used for the calibration of all the spectral features.

2. Time-of-flight secondary ion mass spectroscopy (ToF-SIMS)

The ToF-SIMS analysis of the samples was performed on a TOF.SIMS 5 instrument (IONTOF USA, Inc.) equipped with a Bi_n^{m+} (n = 1–5, m = 1,2) liquid metal ion gun, Cs, and O_2 dual-source ion column for ultralow energy sputtering, and low energy electron flood gun for charge compensation. For the depth profile, a 500 eV Cs^+ sputter ion beam with a 30 nA current was applied to create a $200 \times 200\,\mu m^2$ area. The analysis was performed over a $50 \times 50\,\mu m^2$ area in the center of the sputter crater, which was analyzed by using a pulsed 30 keV, 0.13 pA Bi^+ primary ion beam. The negative ions were collected, and the mass-to-charge ratio was calibrated using C^-, CH^-, CH_2^-, CH_3^-, C_2^-, C_2H^-, and C_3^-. The data were analyzed using ionTOF's SurfaceLab (version 7.3) base data analysis package. The sputtering depths were measured with a profilometer to obtain corresponding sputtering rates of the Si(100) substrate as described in Sec. II C 3, and the thickness of the TiO_2 layer deposited by ALD was measured with ellipsometry as described in Sec. II C 4 to obtain the corresponding sputtering rate.

3. Profilometry

The profilometry analysis was completed with a Bruker Dektak XT profilometer range of 6.5 μm, 3 mg force, and a tip width of 5 μm, run on valley settings. The craters made on Si(100) by ToF-SIMS depth profiling were measured with profilometry, and this measurement was used to establish a sputtering rate for the depth calibration of the Si(100) substrate. The sputter rate used for this calibration of silicon removal was 0.125 nm/s.

4. Ellipsometry

The ellipsometry analysis was performed on a J. A Woolam M-2000VI. A three-layer (film/native oxide/silicon) Cauchy model was used to determine the film thickness of the TiO_2 layer on the OH–Si(100) after 200 cycles of TiO_2 ALD. In the model, the thickness of the native oxide was assumed to be 20 Å. The thickness obtained by ellipsometry was used to calibrate the sputtering rate of the TiO_2 layer in ToF-SIMS depth profile. The sputtering rate for TiO_2 based on this calibration was 0.112 nm/s.

5. Atomic force microscopy (AFM)

The AFM images of the samples were obtained using tapping mode in an Anasys Nano IR2 system. The Bruker gold-coated, microfabricated silicon probes that were ~225 μm long and came pre-mounted on half-washer mounts were used. The images obtained were processed with GWYDDION software (version 2.62).

III. RESULTS AND DISCUSSION

Figure 1 shows the steps followed for the preparation of OH–Si(100), H–Si(100), and FPBA–Si(100). These three surfaces were loaded at the same time in the ALD chamber for each separate run, and 5, 10, 15, 20, 30, 50, and 200 cycles of TDMAT and H_2O were dosed at 130 °C to compare the growth of TiO_2 on all surfaces. After each set of ALD cycles, the samples were loaded into the XPS chamber with minimal exposure to ambient for analysis described in Sec. III A.

A. XPS of growth and non-growth surfaces before and after ALD of TiO_2

Figure 2 shows the B 1s, F 1s, Si 2p, and Ti 2p XPS spectral regions for the FPBA-modified Si(100) surface before and after 5, 10, 20, 30, and 50 ALD cycles of TiO_2. The initial surface [Fig. 2(a)] shows the presence of B 1s feature at around 191.9 eV and F 1s at around 687.1 eV, which correspond to the B and F signal from the FPBA molecule as reported in our previous studies.[19,22] The Si 2p shows the Si bulk signal at 99.4 eV and the higher binding energy peak around 103.0 eV corresponding to Si–O–B bonds.[19] No presence of Ti is recorded on any of the surfaces before the deposition.

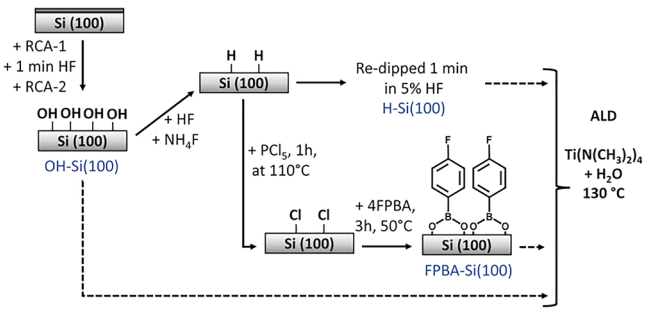

FIG. 1. Steps followed in the preparation of OH-, H-, and FPBA–Si(100) surfaces used in the comparison of TiO_2 growth by ALD.

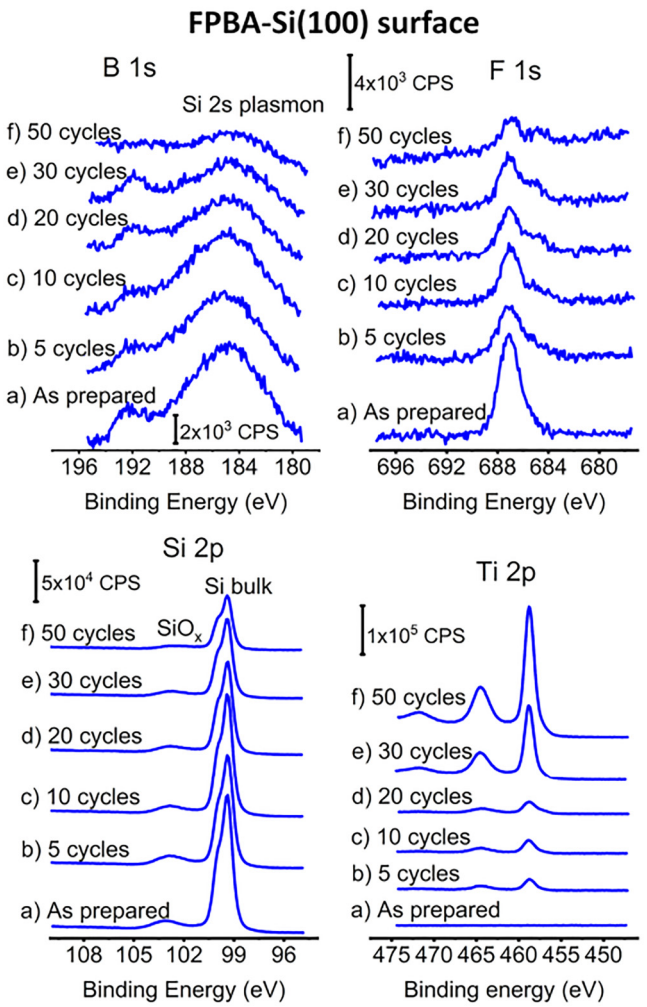

FIG. 2. B 1s, F 1s, Si 2p, and Ti 2p XPS spectral regions of FPBA–Si(100); as prepared (a), and after 5 (b), 10 (c), 20 (d), 30 (e), and 50 (f) ALD cycles of TiO_2.

The relative B/Si coverage obtained after the reaction of FPBA with Cl–Si(100) surface was 0.42 ± 0.01, which corresponds to 74% of a monolayer equivalent to one boron atom per one silicon surface atom based on our previous work.[19] This coverage is actually quite high, given that even the so-called atomically flat H–Si(100) prepared by solution methods is very complex. It corresponds to the saturation on this surface, and no chlorinated species are left on a surface following FPBA modification. A number of possible surface structures and their role in determining the apparent surface FPBA coverage are analyzed elsewhere.[19] It is also important to highlight the FPBA–Si(100) surface stability which will be discussed and compared to that of a H–Si(100) surface.

Following 5–50 ALD cycles onto the FPBA-modified silicon surface [Figs. 2(b)–2(f)], the B 1s signal is clearly observed and decreases substantially only at 50 cycles, and the B 1s peak position is maintained indicating that the chemical environment of boron is not changing substantially. The F 1s signal also clearly decreases, especially by 50 cycles, an additional peak appears at lower binding energy around 684.9 eV which likely corresponds to the interaction of F with Ti, due to the formation of the TiO_2 layer on top of the FPBA molecule. The Si 2p signal also decreases with an increasing number of ALD cycles, which is expected since the surface is being covered by the TiO_2 layer causing the attenuation of the Si signal.[23] The Ti 2p spectral region shows how the Ti 2p signal increases slightly after 5–20 ALD cycles (likely indicating the presence of surface defects) and increases substantially after 50 ALD cycles.

In order to evaluate the selectivity of the TiO_2 deposition, the same procedure was performed on an oxidized (OH-terminated) silicon surface, where both half-cycles of the ALD process are expected to be very efficient. Figure 3 shows the Si 2p and Ti 2p XPS spectral regions for the OH-terminated Si(100) surface before and after 5, 10, 20, 30, and 50 ALD cycles of TiO_2. The initial surface [Fig. 3(a)] shows a substantial oxidation in the Si 2p region at 103.5 eV.[24] After 5–50 cycles [Figs. 2(b)–2(f)], the Si 2p peak intensities decrease with the increasing number of ALD cycles, due to the surface being covered by the growing TiO_2 layer. In the Ti 2p region, the Ti signal intensity increases with the number of ALD cycles, this growth appears to be linear, which is different from what was observed for the FPBA–Si(100) surface. To have a better comparison of the TiO_2 growth on both non-growth surface [FPBA–Si (100)] and growth surface [OH–Si (100)], the Ti 2p/Si 2p ratios, estimated TiO_2 thickness, and selectivity were calculated and discussed further.

Figure S1 in the supplementary material[30] shows the Si 2p and Ti 2p XPS spectral regions of the H–Si(100) before and after 10–50 ALD cycles for comparison. It is important to note that the reactivity of H–Si(100), which is related largely to the defects on this

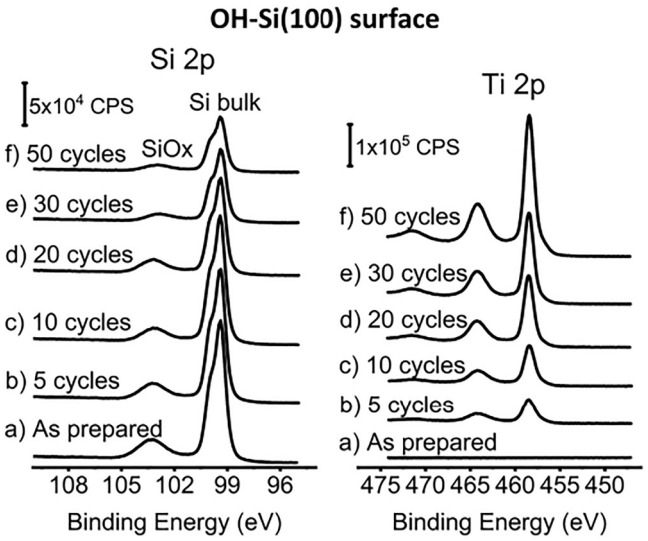

FIG. 3. Si 2p and Ti 2p XPS spectral regions of OH–Si(100) as prepared (a), and after 5 (b), 10 (c), 20 (d), 30 (e) and 50 (f) ALD cycles of TiO_2.

surface,[25,26] is extremely sensitive to the surface preparation procedure. Other studies report a range from exceptionally high surface stability up to 45 ALD cycles[27] to the immediate (albeit slower than on OH-terminated silicon) growth of TiO_2 in similar conditions.[28] The efficiency of the TiO_2 deposition in the studies summarized in this work is between these two extremes and is used largely for comparison with the FPBA-terminated silicon.

Since spectroscopic signature of oxygen is quite distinct in TiO_2, Fig. 4 shows the O 1s XPS spectral region of the OH–Si (100) and FPBA–Si (100) surfaces before and after 5, 10, 20, 30, and 50 ALD cycles. Initially, on both surfaces, a single O 1s peak is observed around 532.0 eV corresponding mostly to the O–Si bonds.[25] After the ALD, noticeable differences on both surfaces are recorded. On the FPBA–Si (100) surface, it is observed that from 5 to 20 cycles the predominant peak is still the one around 532.0 eV. Only a small shoulder at lower binding energy appears following 10 ALD cycles corresponding to the formation of O–Ti bonds.[25] After 30 ALD cycles, this feature becomes dominant in the O 1s spectra. On the OH–Si(100) surface, the O 1s peak at 530.5 eV corresponding to O–Ti is clearly observed even after 5 ALD cycles, this O–Ti peak increases in intensity after 10 cycles and clearly dominates the spectrum after 10 ALD cycles.

This observation indicates that the nucleation of TiO_2 is much faster on the OH–Si(100) surface compared to the FPBA–Si(100) surface, as the latter delays the nucleation of TiO_2 at least up to 20 cycles. Figure S1 in the supplementary material[30] also shows the O 1s peak for the H–Si(100) before and after 10–50 ALD cycles of TiO_2 for comparison.

Based on the O–Ti peak at 530.5 eV measured on each surface, it can be concluded that the nucleation of TiO_2 is slower on the FPBA-modified silicon, especially up to 20 ALD cycles. This can be due to the extra protection that the FPBA-passivated silicon surface provides, as the $(-O-)_2B-(C_6H_4)-F$ functional groups provide steric hindrance that makes the surface inaccessible to react with TDMAT.

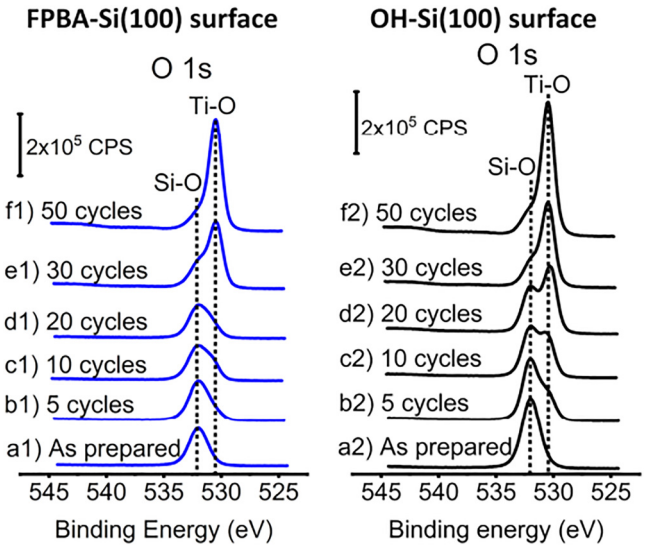

FIG. 4. O 1s XPS spectral region of FPBA–Si(100) (1); as prepared (a1), after 5 (b1), 10 (c1), 20 (d1), 30 (e1), and 50 (f1) cycles of TiO_2 ALD, and OH–Si (100) (2); as prepared (a2), after 5 (b2), 10 (c2), 20 (d2), 30 (e2), and 50 (f2) cycles of TiO_2 ALD.

B. Ti/Si XPS intensity ratios, estimated TiO_2 thickness, and selectivity on the growth and non-growth surfaces

Figure 5 shows the Ti 2p and Si 2p intensity ratios as a function of the number of ALD cycles on the FPBA–Si(100), OH–Si (100), and H–Si(100) surfaces. The OH-terminated Si(100) favors the growth of TiO_2. As can be observed in the graph, the growth of Ti 2p is nearly linear (in fact, the deviation is expected for thicker films, due to the attenuation of Si signal). The FPBA-functionalized Si(100) is the non-growth surface and shows a delay in the growth of TiO_2, this delay is evident up to 20 cycles and then a more linear growth is observed for 30 and 50 ALD cycles. A similar behavior can be observed on the H–Si(100) surface, which shows a delay in the growth of TiO_2 up to 20 cycles and then the growth is linear after 30 and 50 ALD cycles.

The selectivity for the process was calculated using the obtained experimental data on the growth and non-growth surfaces according to Eq. (1),[7]

$$S_x = \frac{R_{GS} - R_{NGS}}{R_{GS} + R_{NGS}}, \quad (1)$$

where S_x is the selectivity after x number of ALD cycles and R represents the experimentally determined amount of deposited material on either GS or NGS. The growth surface for this experiment was OH–Si(100) and the non-growth surface was either H–Si(100) or FPBA–Si(100). In order to perform quantitative selectivity comparison, two approaches can be used. The amount of the material deposited, R, can be determined using the calibrated Ti 2p/Si 2p intensity ratios corrected for appropriate sensitivity factors, as

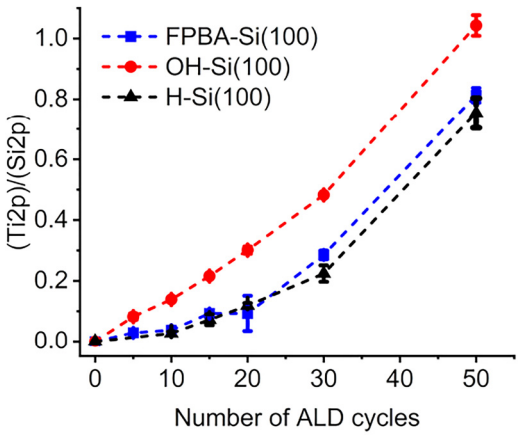

FIG. 5. Ti 2p/Si 2p ratios recorded as a function of the number of ALD cycles.

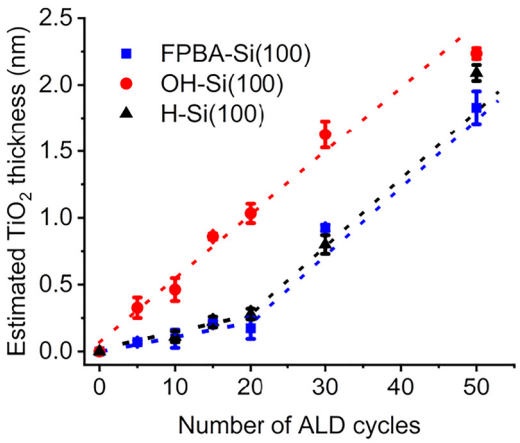

FIG. 6. Estimated TiO_2 thickness (nm) as a function of the number of ALD cycles.

shown in Fig. 5, or using the thickness of the films deposited. The XPS intensity ratio is a formidable approach to perform this estimate; however, it may be complicated by the attenuation of the signal of the underlying substrate, especially if the growth mechanism does not follow a perfect layer-by-layer process but is governed by the surface defects and initial potential island formation of the deposited material. To double-check this, the second approach was also used. Figure 6 plots the estimated thickness of the TiO_2 film deposited on different surfaces as a number of ALD cycles. It shows the estimated TiO_2 thickness calculated from Eq. (2),[28]

$$d_{TiO_2} = -\lambda_{TiO_2} \ln\left(\frac{I_{Si}}{I_{Si,0}}\right), \tag{2}$$

where d_{TiO_2} is the thickness of the TiO_2 layer, λ_{TiO_2} is the photoelectron mean free path in TiO_2, and $I_{Si,0}$ and I_{Si} are the Si 2p peak intensities before and after ALD. A mean free path of 2 nm for the Si 2p electron passing through the TiO_2 overlayer was used. The estimated TiO_2 thickness was calculated for the FPBA–, OH–, and H–Si (100) surfaces for different numbers of ALD cycles.

This method also provides the best results for a true layer-by-layer ALD process, and the OH-terminated Si(100) surface shows a nearly perfect linear growth of TiO_2 with an increasing number of ALD cycles with an $R^2 = 0.98$. On the other hand, the FPBA–Si(100) shows a slower TiO_2 growth, which results in less than 0.25 nm deposited in total up to 20 ALD cycles, yielding a more linear behavior compared to the one shown in Fig. 5 for the same regime (0–20 cycles) of the deposition process. After 30 and 50 cycles, the TiO_2 growth rate increases and shows a linear growth with basically the same slope as that describing the behavior of OH–Si(100) surface, indicating that the selectivity is lost at this point. To compare with a standard non-growth surface, the H–Si(100) was also considered. After 20 cycles, the growth of TiO_2 is similar to that on the FPBA–Si(100) surface, and after 30 and 50 cycles the growth of TiO_2 becomes linear with a slope similar to that on the OH–Si(100) surface. This shows that the growth of TiO_2 on the H–Si(100) surface is similar to the growth of TiO_2 on the FPBA–Si(100). It is important to emphasize that H–Si(100) was re-dipped in HF before loading in the ALD chamber to guarantee that it has minimal oxidation, while the FPBA-Si(100) surface did not need any additional treatment steps.

Table I summarizes this comparison in terms of selectivity based on both approaches. The left three columns report the selectivity based on the XPS intensity ratio, while the right three use estimated film thickness. This comparison shows that the selectivity calculated for FPBA- and H-Si surfaces is similar, approximately 0.6, regardless of the approach used to calculate this parameter, up to 20 ALD cycles. Then, as the number of cycles increases, the selectivity decreases until it is lost after 50 cycles.

It is important to note that these seemingly modest selectivity numbers are on par with and even better than the ones reported previously for practical applications. For example, the selectivity between 0.28 for 10 cycles[28] and 0.72 for up to 75 cycles[29] was reported for the combination of oxidized and H-terminated silicon in a deposition process involving half-cycles of $TiCl_4$ and water. However, the FPBA–Si surface has the advantage of being much more stable in ambient conditions. As summarized in Figs. S2 and S3 in the supplementary material,[30] H–Si(100) exhibits substantial oxidation within 2 h, while FPBA–Si(100) surface maintains its structure for at least 48 h, as suggested by XPS.

TABLE I. Comparison of the selectivity of FPBA–Si(100) and H–Si(100) (non-growth surfaces) compared to OH–Si(100) (growth surface) calculated from Eq. (1) using Ti 2p/Si 2p ratios obtained with XPS and calculated from Eq. (2) using the estimated TiO_2 thickness.

Selectivity of non-growth surfaces calculated with Ti 2p/Si 2p XPS intensity ratios [Eq. (1)]			Selectivity of non-growth surfaces calculated from apparent film thickness [Eq. (2)]		
Cycles	FPBA–Si(100)	H–Si(100)	Cycles	FPBA–Si(100)	H–Si(100)
5	0.60 ± 0.10	—	5	0.60 ± 0.03	—
10	0.60 ± 0.10	0.60 ± 0.02	10	0.70 ± 0.02	0.60 ± 0.11
15	0.40 ± 0.01	0.50 ± 0.10	15	0.60 ± 0.04	0.60 ± 0.04
20	0.50 ± 0.20	0.40 ± 0.04	20	0.70 ± 0.11	0.60 ± 0.04
30	0.30 ± 0.02	0.40 ± 0.05	30	0.30 ± 0.03	0.30 ± 0.06
50	0.10 ± 0.02	0.20 ± 0.10	50	0.10 ± 0.03	0.03 ± 0.01

Maintaining reasonable selectivity for at least 20 cycles of effective ALD process provides a target for 2 nm technology that does not require additional steps or back-etching procedures. At the same time, given that the initial silicon wafer preparation involves solution steps, using additional solution processing before the start of the deposition and patterning process may be easily handled by the manufacturers.

Thus, it appears that FPBA–Si(100) is just as efficient as the H–Si(100) surface in its role as an NGA. However, it also has a number of advantages. FPBA–Si(100) can be easily handled in ambient conditions and is exceptionally resistant to further oxidation, making it an excellent starting platform for area-selective deposition. It is passivated by the Si–O–B bonds and is protected with the $(–O–)_2B–(C_6H_4)–F$ functional groups that apparently delay the growth of TiO_2.

C. ToF-SIMS depth profile on growth and non-growth surfaces

To further confirm the TiO_2 thickness estimated from XPS and complement the obtained chemical information using F and B as spectroscopic labels, ToF-SIMS depth profile was used to analyze the OH– and FPBA–Si(100) surfaces after 50 and 200 ALD cycles. The 50 and 200 cycles were chosen as representative points, since these samples exhibited consistent and reliable properties determined by combining ToF-SIMS, ellipsometry, and profilometry measurements and also in both cases the films deposited were very smooth according to AFM. AFM measurements shown in the supplementary material (Fig. S4),[30] after 50 cycles a uniform layer is deposited on both surfaces, with RMS roughness of 0.23 nm for the FPBA–Si(100) surface and RMS roughness of 0.25 nm for the OH–Si(100) surface.

On the FPBA–Si(100) surface after 50 ALD cycles [Fig. 7(a)], the interface between titania and silicon is observed at approximately 2.9 nm in depth, if the depth is calibrated as described in Secs. II C 3 and II C 4 and the appropriate sputtering rates are obtained to convert the sputtering time scale into the depth scale. Right at the interface, F^- and B^- are present, and a small shift of about 6 Å between F^- and B^- negative ion depth profiles is observed, which corresponds to the length of the FPBA molecule according to the computational models reported in our previous studies.[19] The FPBA molecule binds to the Si surface forming B–O–Si bonds, which was confirmed with XPS; therefore, the

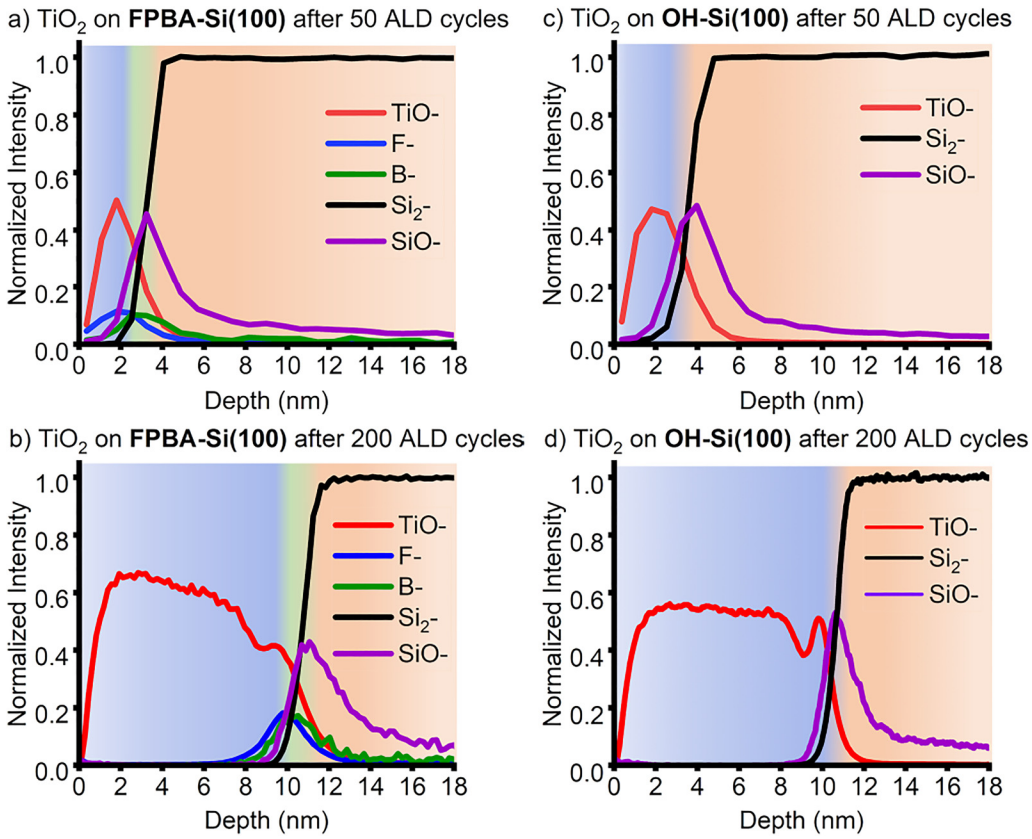

FIG. 7. ToF-SIMS depth profile showing the intensity of the TiO^-, F^-, B^-, Si_2^-, and SiO^- ions vs depth of (a) FPBA–Si(100) after 50 cycles and (b) FPBA–Si(100) after 200 cycles. The intensity of TiO^-, Si_2^-, and SiO^- ions vs depth of (c) OH–Si (100) after 50 cycles and (d) OH–Si(100) after 200 cycles. All the intensities were normalized to Si_2^- at saturation.

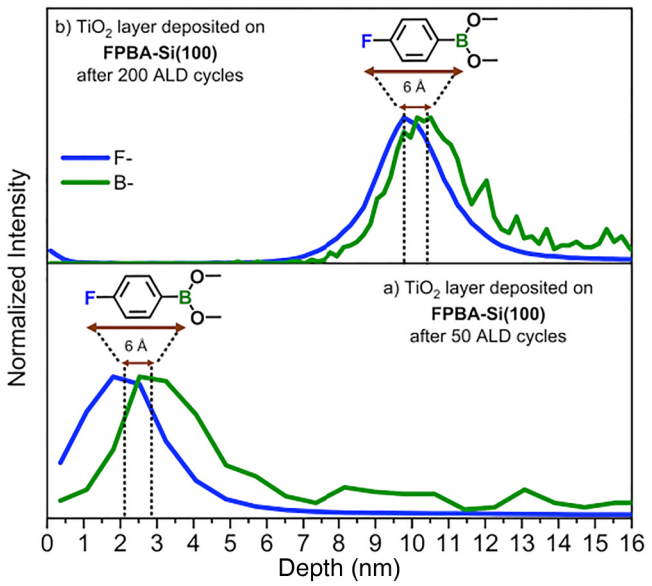

FIG. 8. ToF-SIMS depth profile showing the intensity of the F^- and B^- ions vs depth of FPBA–Si(100) after 50 cycles (a) and FPBA–Si(100) after 200 cycles (b).

SiO- fragment which is also at the interface corresponds to the O–Si bond formed after the FPBA reaction.

After 200 ALD cycles on the FPBA–Si(100) surface, the interface between titania and silicon is recorded at approximately 10.5 nm in depth, and it is also observed that the SiO^-, F^- and B^- ions remain at the interface at their original positions, as a small shift of about 6 Å between F^- and B^- negative ions also remains in place. This observation is consistent with the FPBA molecule staying at the interface without any of its constituents diffusing into the TiO_2 layer. The difference in depth location for F and B elements is also fully consistent with the entire fluorophenylboronic functionality being intact.

On the OH–Si(100) surface after 50 cycles, it is observed that the interface between titania and silicon is just above 3.5 nm in depth (reflecting nearly the same TiO_2 thickness as that estimated in XPS experiments). For this sample, SiO^- ion at the interface corresponds to the oxidized silicon surface as confirmed with XPS with the peak at ~103 eV. Whereas after 200 cycles on the OH–Si (100) surface, the interface between titania and silicon is at approximately 10.6 nm.

Thus, following 50 cycles of ALD onto FPBA–Si(100) surface, the thickness of TiO_2 according to ToF-SIMS measurements is ~2.9 nm, and the TiO_2 layer on the OH–Si(10) surface is ~0.6 nm thicker, which matches with the results obtained for the estimated TiO_2 thickness calculated with Eq. (2).

After 200 ALD cycles, the TiO_2 thickness on both FPBA- and OH-Si(100) surfaces appears to be similar. At this point, the selectivity is completely lost, the interface is buried, and the accuracy of pinpointing it precisely is limited. However, it is more important for the thicker TiO_2 layer to interrogate the structure of the interface between the oxide and silicon substrate. As was mentioned above, B and F are used as spectroscopic labels in XPS and ToF-SIMS experiments, providing information about the intactness and stability of the molecule at the interface.

Figure 8 provides a zoomed-in comparison of the F^- and B^- ions intensity versus depth obtained by ToF-SIMS depth profile of the FPBA–Si(100) surface after 50 and 200 TiO_2 ALD cycles. The 4-fluorophenylboronic functionality remains at the interface following the process and the distance between F^- and B^- labels is maintained at both depths. This set of measurements also suggests that this chemical group remains intact, as a clear and reproducible shift of 6 Å between F^- and B^- is observed. The theoretically predicted distance between B^- and F^- in the FPBA molecule after the attachment to the Si(100) is 5.7 Å as calculated from the computational models reported in our previous studies.[19] To further confirm the intactness of the $(-O-)_2B-(C_6H_4)-F$ functional group, the CF^-, $FC_6H_4BO_2^-$, and $C_6H_4^-$ fragments were also identified at the interface of the TiO_2 layer and the FPBA-modified Si(100) as shown in Fig. S5 in the supplementary material.[30] Although some of these fragments exhibit very low intensity and thus low signal-to-noise ratios, it is apparent that the CF^- depth profile largely coincides with the F^- depth profile, confirming the presence of the C–F bond at the TiO_2/Si(100) interface, consistent with the XPS observations that were discussed above for the sample prepared by 50 cycles of ALD. On the other hand, the peak position of the B^- appears to precede the small signals corresponding to the aromatic ring and to the entire molecular fragment ($FC_6H_4BO_2^-$), thus confirming the high sensitivity of the ToF-SIMS technique and reinforcing the hypothesis that the 4-fluorophenylboronic functionality remains intact following the loss of selectivity of the functionalized surface and eventual TiO_2 deposition.

This behavior and stability may be important not only to the use of FPBA-modified surfaces as NGA, but also brings up an important issue of modifying electronic and physical properties of the interfaces obtained on SMI-modified substrates, for example, by thermal treatment, following the eventual loss of selectivity. Given the differences in electronic structure of fluorine in exposed and buried FPBA functionality suggested by XPS, it remains to be seen if fluorine presence can influence the chemical protection in deposition processes and if thermal stability of the buried interface may be important in ultra-shallow doping approaches; however, these questions will be a subject of further investigations.

IV. CONCLUSIONS

FPBA–Si(100) surface delayed the deposition of TiO_2 up to 20 cycles with a selectivity of up to 70% compared to the GA of OH–Si(100) in the ALD process based on TDMAT/water. This behavior is very similar to a traditional H–Si(100) surface acting as a NGA in the same deposition scheme, but the FPBA–Si(100) substrate exhibited exceptional stability in ambient, being stable for days compared to hours or even minutes for H–Si(100).

F^- and B^- served as tracking labels in XPS and ToF-SIMS investigations to calculate coverage and evaluate the intactness and stability of the 4-fluorophenylboronic functional group at the interface with silicon following the ALD process. It appears that the entire chemical functionality remains intact in this system, which may be

very important not only for the use of FPBA–Si(100) as an NGA, but also in designing interfaces with tunable electronic properties.

ACKNOWLEDGMENTS

This work was partially supported by the National Science Foundation (NSF) (Nos. CMMI-2035154 and CMMI-2225900) and by the U.S. Department of Energy's Office of Energy Efficiency and Renewable Energy (EERE) under the Solar Energy Technologies Office (No. DE-EE0010249). The XPS and ToF-SIMS experiments were performed with the instrument sponsored by the National Science Foundation under Grant Nos. CHE-1428149 and DMR-2116754. Selected studies were also supported by the Chemours Company.

AUTHOR DECLARATIONS

Conflict of Interest

The authors have no conflicts to disclose.

Author Contributions

Dhamelyz Silva-Quinones: Conceptualization (equal); Data curation (lead); Formal analysis (equal); Investigation (lead); Methodology (equal); Validation (equal); Visualization (equal); Writing – original draft (lead); Writing – review & editing (equal). **John R. Mason:** Data curation (equal); Formal analysis (equal); Investigation (equal); Writing – review & editing (equal). **Robert Norden:** Data curation (equal); Investigation (equal); Writing – review & editing (equal). **Andrew V. Teplyakov:** Conceptualization (equal); Data curation (equal); Formal analysis (equal); Funding acquisition (equal); Investigation (equal); Methodology (equal); Project administration (equal); Resources (equal); Supervision (equal); Writing – review & editing (equal).

DATA AVAILABILITY

Spectroscopic and microscopic data used in this study are available from the corresponding author upon reasonable request.

REFERENCES

[1]*Convergence of More Moore, More Than Moore, and Beyond Moore*, edited by S. Deleonibus (Jenny Stanford Publishing Pte. Ltd., Singapore, 2020), Vol. 4.
[2]G. N. Parsons and R. D. Clark, Chem. Mater. **32**, 4920 (2020).
[3]A. J. M. Mackus, M. J. M. Merkx, and W. M. M. Kessels, Chem. Mater. **31**, 2 (2019).
[4]J. Zhang, Y. Li, K. Cao, and R. Chen, Nanomanuf. Metrol. **5**, 191 (2022).
[5]A. Mameli, B. Karasulu, M. A. Verheijen, A. J. M. Mackus, W. M. M. Kessels, and F. Roozeboom, ECS Trans. **80**, 39 (2017).
[6]S. Yasmeen, S. W. Ryu, S. H. Lee, and H. B. R. Lee, Adv. Mater. Technol. **8**, 2200876 (2023).
[7]J. Yarbrough, A. B. Shearer, and S. F. Bent, J. Vac. Sci. Technol., A **39**, 021002 (2021).
[8]X. Jiang and S. F. Bent, J. Phys. Chem. C **113**, 17613 (2009).
[9]T. L. Liu, L. Zeng, K. L. Nardi, D. M. Hausmann, and S. F. Bent, Langmuir **37**, 11637 (2021).
[10]D. Bobb-Semple, L. Zeng, I. Cordova, D. S. Bergsman, D. Nordlund, and S. F. Bent, Langmuir **36**, 12849 (2020).
[11]R. A. Nye, K. Van Dongen, D. De Simone, H. Oka, G. N. Parsons, and A. Delabie, Chem. Mater. **35**, 2016 (2023).
[12]N. Poonkottil, H. Rijckaert, K. Rajendran, R. R. Petit, L. I. D. J. Martin, D. Van Thourhout, I. Van Driessche, C. Detavernier, and J. Dendooven, Adv. Mater. Interfaces **10**, 2201934 (2023).
[13]E. Frederick, K. J. Dwyer, G. T. Wang, S. Misra, and R. E. Butera, J. Phys.: Condens. Matter **33**, 444001 (2021).
[14]A. Mameli and A. V. Teplyakov, Acc. Chem. Res. **56**, 2084 (2023).
[15]T. R. Leftwich, M. R. Madachik, and A. V. Teplyakov, J. Am. Chem. Soc. **130**, 16216 (2008).
[16]F. Tian, Y. Cui, and A. V. Teplyakov, J. Phys. Chem. C **118**, 502 (2014).
[17]F. Tian, D. F. Taber, and A. V. Teplyakov, J. Am. Chem. Soc. **133**, 20769 (2011).
[18]Y. Cui, F. Tian, F. Gao, and A. V. Teplyakov, J. Phys. Chem. C **118**, 26721 (2014).
[19]D. Silva-Quinones, R. E. Butera, G. T. Wang, and A. V. Teplyakov, Langmuir **37**, 7194 (2021).
[20]W. Kern, J. Electrochem. Soc. **137**, 1887 (1990).
[21]A. Bansal, X. Li, S. I. Yi, W. H. Weinberg, and N. S. Lewis, J. Phys. Chem. B **105**, 10266 (2001).
[22]C. Byron, D. Silva-Quinones, S. Sarkar, S. C. Brown, S. Bai, C. M. Quinn, Z. Grzenda, M. S. Chinn, and A. V. Teplyakov, Chem. Mater. **34**, 10659 (2022).
[23]A. C. Bronneberg, C. Höhn, and R. Van De Krol, J. Phys. Chem. C **121**, 5531 (2017).
[24]S. Rani, C. Byron, and A. V. Teplyakov, J. Chem. Phys. **152**, 134701 (2020).
[25]T. Parke, D. Silva-Quinones, G. T. Wang, and A. V. Teplyakov, ChemPhysChem **24**, e202200724 (2023).
[26]R. A. Nye, S. K. Song, K. Van Dongen, A. Delabie, and G. N. Parsons, Appl. Phys. Lett. **121**, 082102 (2022).
[27]R. C. Longo, S. McDonnell, D. Dick, R. M. Wallace, Y. J. Chabal, J. H. G. Owen, J. B. Ballard, J. N. Randall, and K. Cho, J. Vac. Sci. Technol., B **32**, 03D112 (2014).
[28]R. Methaapanon and S. F. Bent, J. Phys. Chem. C **114**, 10498 (2010).
[29]J. W. J. Clerix, G. Dianat, A. Delabie, and G. N. Parsons, J. Vac. Sci. Technol., A **41**, 032406 (2023).
[30]See supplementary material for additional XPS studies, surface stability tests, and AFM images of the starting surfaces and the same surfaces following ALD.